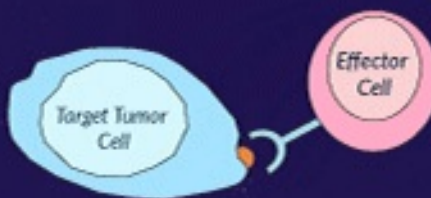


ADVERTISEMENT

Does your *in vitro* cell killing assay translate *in vivo*?



Download our Immu

Download Now

[plos.org](#)

[create account](#)

[sign in](#)



[Publish](#)

[About](#)

OPEN ACCESS PEER-REVIEWED

RESEARCH ARTICLE

# The Scale-Free Dynamics of Eukaryotic Cells

Miguel A. Aon , Marc R. Roussel, Sonia Cortassa, Brian O'Rourke, Douglas B. Murray, Manfred Bec

Published: November 4, 2008 • <https://doi.org/10.1371/journal.pone.0003624>

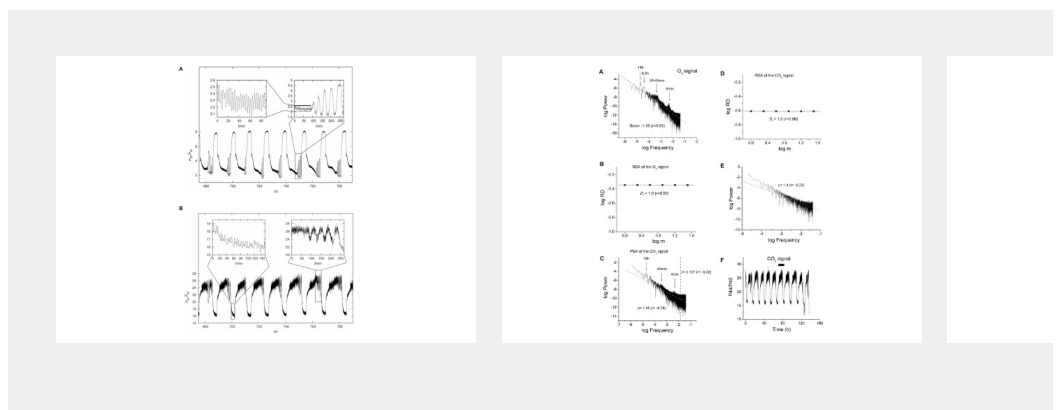
Article	Authors	Metrics	Comments

Reader Comments (0)

Media Coverage

Figures

## Figures



# Abstract

Temporal organization of biological processes requires massively parallel a synchronized time-base. We analyzed time-series data obtained from oscillatory outputs of *Saccharomyces cerevisiae* and isolated cardiomyocytes using Relative Dispersional (RDA) and Power Spectral (PSA) analyses. The broad frequency distributions and evidence for long-term memory dynamics. Moreover RDA and PSA showed that the bioenergetic dynamics systems show fractal scaling over at least 3 orders of magnitude, and obeys an inverse power law. Therefore we conclude that in *S. cerevisiae* cardiomyocytes the dynamics are scale-free *in vivo*. Applying RDA to data generated from an *in silico* model of mitochondrial function indicate that in cardiomyocytes the underlying mechanisms regulating the scale-free dynamics are similar. We validated this finding *in vivo* using single cells, and after the mitochondrial inner membrane anion channel with 4-chlorodiazepam-induced oscillation of NAD(P)H and reactive oxygen species (ROS) can be at least in evolutionarily distant species. Taken together these data strongly suggest that the generation of ROS, coupled to redox cycling, driven by cytochrome *c* and mitochondrial processes, are at the core of the observed rhythmic dynamics. We argue that the operation of scale-free bioenergetic dynamics has a fundamental role to integrate cellular function, while providing a flexible, responsive to the environment.

**Citation:** Aon MA, Roussel MR, Cortassa S, O'Rourke B, Murray D et al. (2008) The Scale-Free Dynamics of Eukaryotic Cells. PLoS ONE 3(12): e3624. doi:10.1371/journal.pone.0003624

**Editor:** Eshel Ben-Jacob, Tel Aviv University, Israel

**Received:** July 24, 2008; **Accepted:** October 11, 2008; **Published:** December 12, 2008

**Copyright:** © 2008 Aon et al. This is an open-access article distributed under the terms of the Creative Commons Attribution License, which permits unrestricted use, distribution, and reproduction in any medium, provided the original author(s) and source are credited.

**Funding:** NIH grant R37-HL54598. The funding agency had no role in the design, data collection and analysis, decision to publish, or preparation of the manuscript.

**Competing interests:** The authors have declared that no competing interests exist.

## Introduction

In their long evolutionary history, unicellular and multicellular organisms have achieved the two divergent, although complementary, goals of matching their internal environments with the periodicities of the external world.

of annual, seasonal, daily and tidal rhythms), and optimizing for tolerance to perturbation [1], [2], [3], [4], [5]. As a result, living systems have developed internal coordination to maintain spatial and temporal organization from microscopic to the macroscopic levels [1], [4], [6], [7], [8], [9]. For instance, energy, biosynthetic pathways, assembly of multimeric proteins, membrane organelles, stress responses, cell differentiation, migration and cell cycle are temporally organized on many time scales simultaneously [10], [11]. Complex biological timing requires more than circadian organization. In the ultradian domain (i.e. faster time scales where clocks cycle many times per day) is essential. Examined more closely, it is evident that additional clocks exist. For instance, a circadian clock provides a time base on a scale of hours, while rhythms or oscillations measured in minutes [15], [16], seconds [17], [18] are abundant in biological systems. This leads to the central but enigmatic question of biological timekeeping: whether synchrony occurs between these clocks and how function correlates across different time domains.

The concept of scaling [11], [19], [20], [21], [22] provides a theoretical framework to address questions about interactions and correlations across different spatial and temporal scales. These theoretical concepts as applied to the topological architecture of biological networks showed their non-random scaling properties [23], [24]. Geometric fractals have been successfully used to describe spatial and temporal organization, respectively, across many levels of organization, owing to their intrinsic self-similar scaling properties [21], [25]. A recent example is given by the analysis of membrane potential ( $V_m$ ) noise and the spatial organization of the mitochondrial network [18]. These findings, which complement other observations of scale invariance of cardiac function [26], [27], [28], provide fundamental insights into describing and diagnosing pathological conditions [29], [30], [31]. The synchronization of multioscillatory states, implying controlled chaotic dynamics [32], [33], [34] appear to be essential properties governing the regulation of metabolism and transcription across a population of single celled organisms. For continuous cultures of *S. cerevisiae* [13], [35].

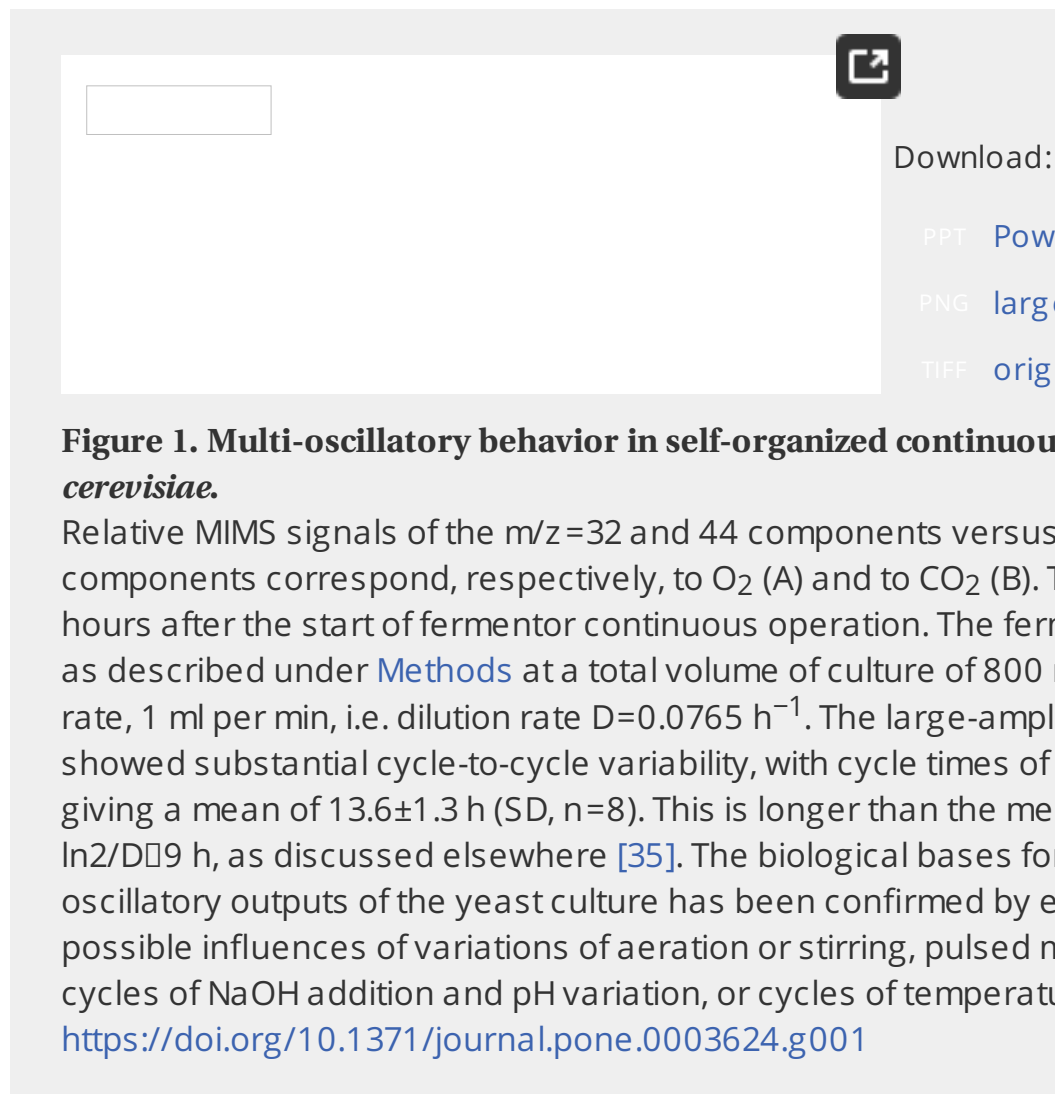
Hence, in the present work, we sought to determine if there are correlations between biological organization and fractal scaling of bioenergetics in two eukaryotic cellular systems, i.e., baker's yeast and cardiomyocytes, utilizing precise physiological and pathological conditions. Using a combined experimental and computational approach we demonstrate that the observed multioscillatory behavior exhibited by yeast and cardiac cells are scale-free. The results suggest a mechanism of biological timekeeping based on fractal scaling of periodic oscillations, which is characterized by a large number of frequencies as outputs on multiple time scales.

## Results

### Multi-oscillatory behavior and fractal dynamics in yeast

It has previously been observed that yeast can produce multiple frequencies of oscillation continuously under precisely controlled conditions. Figure 1 shows

dissolved oxygen (Fig. 1A) and carbon dioxide (Fig. 1B) concentration time series. Periods of  $\approx 13$  h,  $\approx 40$  min and  $\approx 4$  min can be detected (see text). The lower limit is most probably the minimum sampling frequency imposed by the measurement system.

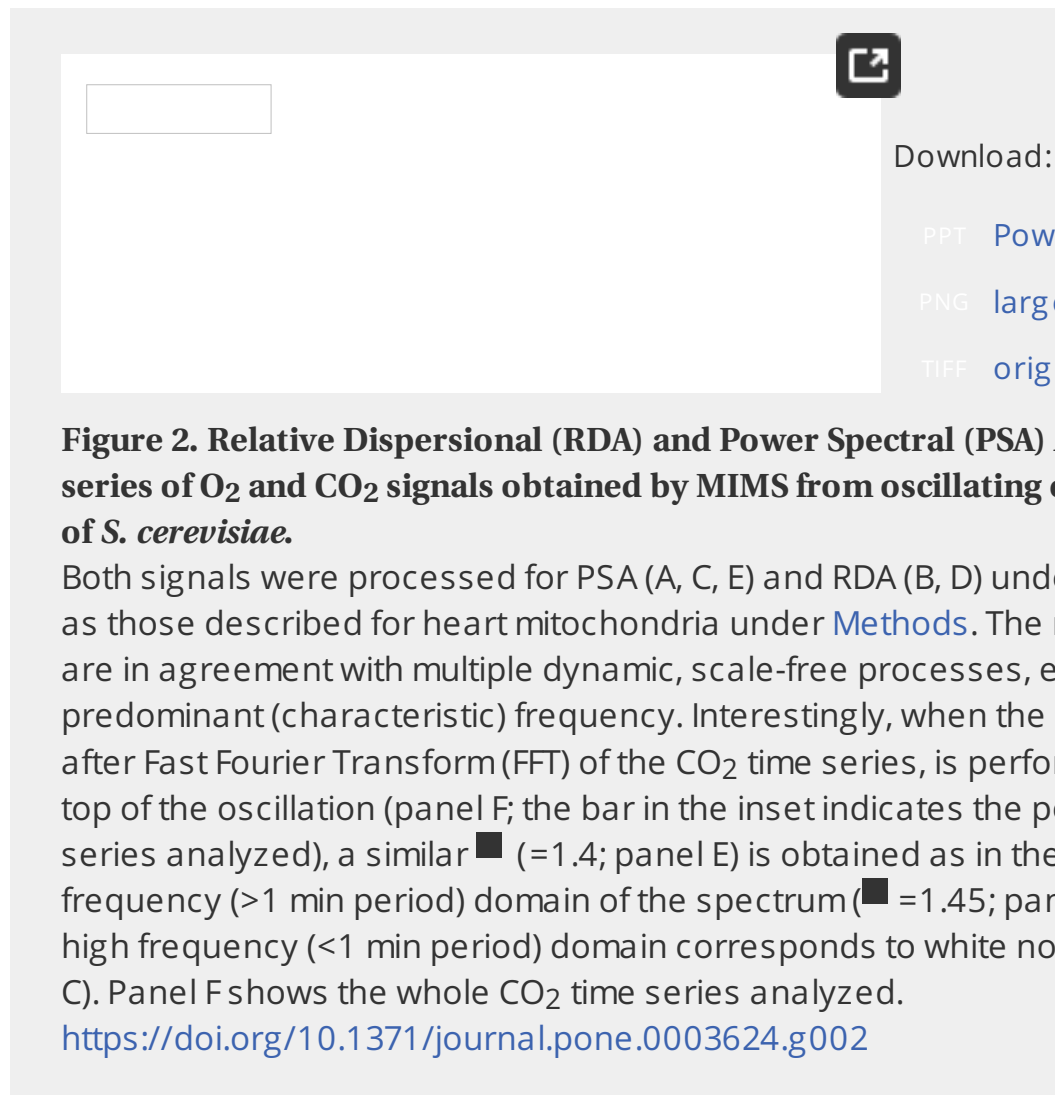


It has also been shown that the trajectory described by this dynamical system can be represented as a chaotic attractor [35], as the leading Lyapunov exponent is  $0.752\pm 0.004\text{ h}^{-1}$  (95% confidence), indicating sensitivity to initial conditions. Chaotic performance also comes from other work [36], [37], [38].

Closer examination of a part of a single long-period cycle (Fig. 1) shows that the  $\approx 40$  min (Fig. 1B) as a super-imposed series of bursts in each dominant  $\approx 13$  h cycle. The observed variability of this rhythm [35] is probably due in part to superimposed faster and slower rhythms, although analysis of the period of ultradian clock oscillations provides evidence for its inherently chaotic control [37]. On this time scale, the  $CO_2$  concentration is reciprocally related to dissolved  $O_2$ , indicating that the  $CO_2$  production is the major process in this aerobic culture.

We processed the  $O_2$  (Fig. 2A and 2B) and  $CO_2$  (Fig. 2C–E) time series using Rescaled Range Analysis (RDA). RDA revealed that the observed multioscillatory dynamics correspond to fractals, as can be judged by the perfect correlation between oscillations in the 13 min and 4 min time domains. The double log plots depicted in Figure 2 show an inverse power relationship with a fractal dimension,  $D_f (=1.0)$  implying self-similarity with scale (i.e., the time series looks *statistically* similar at all scales). The observed inverse power law behavior is consistent with long-term memory in the time series.

and suggests fractal dynamics of processes on different time scale (several hours) [21], [25].



PSA also indicates an inverse power law proportional to  $1/f^\beta$ . This is characteristic of time series exhibiting self-similar scaling by RDA. The value of  $\beta = 1.4$  for the O<sub>2</sub> signal (Fig. 2A) is close to that characteristic of colored noise, and that expected for chaotic time series. The PSA of the CO<sub>2</sub> signal was different with the results obtained with the O<sub>2</sub> power spectrum. For the CO<sub>2</sub> signal a value of  $\beta \approx 1.45$  at frequencies higher than 0.016 Hz (1 min oscillation) and below this frequency only white noise was recovered, i.e.  $\beta \approx 0$  (Fig. 2C). When analyzed the top of the CO<sub>2</sub> oscillatory response (Fig. 2F) a similar power spectrum (Fig. 2E) was obtained, arguing that this part of the signal is rich in high frequency. The frequency richness of the CO<sub>2</sub> power spectrum beyond the most characteristic frequencies is  $\approx 14$  h,  $\approx 40$  min,  $\approx 4$  min.

In order to further demonstrate the statistical fractal nature of the time series, we simulated a time series that captured two essential features: *i*) similar to the one determined experimentally; and *ii*) the inverse relationship between power and frequency which is at the origin of the inverse power law determined experimentally (Fig. 7 of [18], and its associated text about *Origins of the inverse power law*). The simulated time series (see M&M), similar to the experiment (compared with the one tested if: *i*) the addition of the three separate time series, corresponding to the three different time scales, into one time series allowed us to reproduce the results obtained by the experiment. There is any discernible (geometric) self-similarity in the unified time



Here, we analyze simultaneously the  $\Delta F_m$  or NADH and ROS time series in cardiomyocytes by two photon microscopy with high ( $\approx 100$  ms) temporal resolution. We were probed with two different sensors, CMH<sub>2</sub>DCF, for H<sub>2</sub>O<sub>2</sub> [43] and a superoxide free radical, O<sub>2</sub><sup>·-</sup> [44]. CMH<sub>2</sub>DCF was assayed in parallel with a ROS sensor, while MitoSox was monitored together with the cell's autofluorescence. Both  $\Delta F_m$  and ROS signals exhibit scale-free dynamic behavior, as expected for coupled oscillators [18]. Shown in Figure 4 are the time series of both sensor signals from a mitochondrial network (Fig. 4 A–E) or an individual mitochondrion (Fig. 4 F–J). By RDA and PSA (Fig. 4 A–C, and F–H) we show that mitochondria in cardiomyocytes also exhibit, as in the evolutionarily distant yeast, a scale-free temporal organization. Both  $\Delta F_m$  and ROS signals are highly correlated according to PSA (Fig. 4E) and RDA (Fig. 4I, top trace). This correlation is also observed in mitochondria (Fig. 4F–H) as shown by increased white noise behavior in the power spectrum (Fig. 4J) and lower correlation by RDA (Fig. 4I, lower trace). In the millisecond time scale (*ca.* 450 ms period) both signals exhibit a scale-free relationship [43].

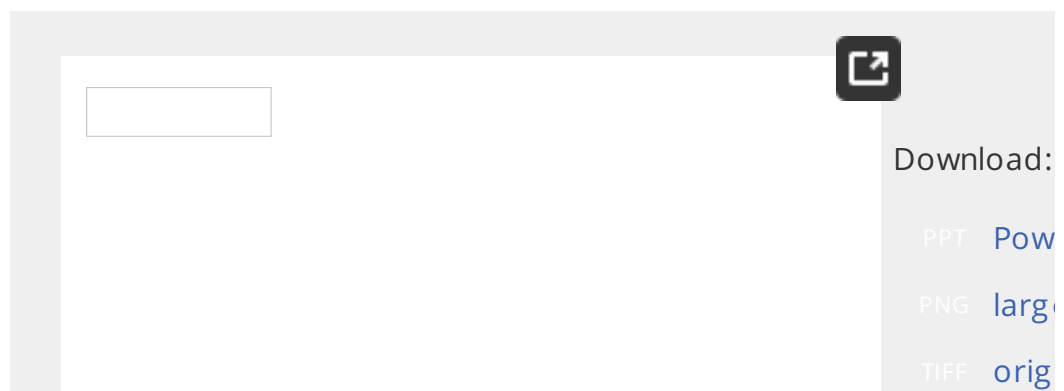


**Figure 4. RDA and PSA of  $\Delta F_m$  and Reactive Oxygen Species (ROS) time series from a mitochondrion or the mitochondrial network of cardiomyocytes.**

Time series of the mitochondrial network within the oscillating mitochondria (A–D) or of a mitochondrion outside the cluster (F–H) were analyzed in isolated ventricular cardiomyocytes loaded with 100 nM TMRM, 100 nM CMH<sub>2</sub>DCF, and 2  $\mu$ M CMH<sub>2</sub>DCF, a ROS sensor, and imaged by two photon microscopy (100 ms time resolution). The results obtained from a stack of 3,050 images (100 frames) are shown in this panel. This panel shows the time series from the mitochondrial network (A–D) and from an individual mitochondrion (F–H) of a cardiomyocyte loaded with TMRM and CMDCF and imaged as described in the caption of panels A–C and F–H, the  $\Delta F_m$  and ROS signals from the mitochondria (A–C) or an isolated mitochondrion (F–H) are depicted at increasing magnification; notice the degree of self-similarity of both signals as confirmed by PSA (E) and RDA (I) analyses of the time series. Parallel to the expected phase relationship between the TMRM and CM-DCF signals, the time series of TMRM or CM-DCF fluorescence was subjected to Fractal Dimension (FD) analysis (see the [Methods](#) section). The power spectrum was obtained from the time series of the TMRM or CM-DCF signal as the double log plot of the amplitude (power) versus the frequency. This relationship obeys a homogeneous power law ( $P \propto f^{-\beta}$ , where  $\beta$  is the spectral exponent) and is statistically self-similar. The PSA reveals a scale-free oscillation in normally polarized mitochondria with a spectral exponent of  $\beta \approx 1.5$ .

while a random process (white noise) gives a  $D_f = 0$  meaning that the relationship between the amplitude and the frequency in a random process corresponds to pink or brown noise, respectively. The inverse power spectrum arises from the coupling of frequency and amplitude in a statistical sequence. I) RDA: A log-log plot of the relative dispersion of the fluorescence distribution obtained at increasing values of the parameter,  $m$  (see also the [Methods](#) section) gives a fractal dimension of 1.0, under “physiological” conditions (panel I, top trace). A completely random process gives  $D_f = 1.5$ . The data obtained from RDA was subjected to linear regression and the slope calculated ( $D_f = 1 - \text{slope}$ ). Randomization of a series of the TMRM fluorescent signal gives a value of  $D_f$  close to 1.0, as shown in the power spectrum shown in panel J, as opposed to a  $D_f = 1.8$  in the non-randomized signal obtained from the mitochondrial network (E). The spectral exponent is consistent with long-range correlations that, after signal randomization, are lost, with loss of correlation properties  $D_f = 0.3$  ( $\approx 0$ ) (J).  
<https://doi.org/10.1371/journal.pone.0003624.g004>

The statistical fractal nature of the ROS signal was further confirmed using a sensor of  $O_2^{\cdot-}$  MitoSox, the ROS species that our experimental data favors as the intracellular messenger between mitochondria [43], [44]. In this case the ROS signal was analyzed concomitantly with the cell's autophagy signals behaved as statistical fractals (Fig. 5B). The MitoSox fluorescence increases in a stepwise fashion during mitochondrial oscillations (Fig. 5A). In two dimensions,  $D_f \approx 1.0$ , obtained after RDA is clearly different from uncorrelated noise obtained from the image background (Fig. 5B). This result is consistent with long-range memory in agreement with the statistical fractal dynamics of the ROS signal.

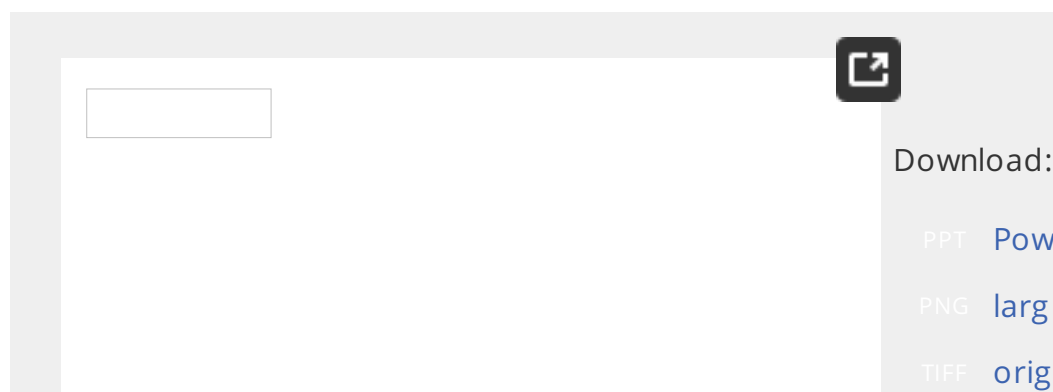


**Figure 5. RDA of ROS and NADH fluorescence time series from the mitochondrial network of cardiomyocytes.**

Freshly isolated cardiomyocytes were loaded with 2  $\mu\text{M}$  MitoSox at 37°C, and imaged by two photon microscopy (120 ms time resolution). Panel A shows a representative result for MitoSox and NADH fluorescence of a stack of 2,200 frames. Notice the ladder-like increase in the MitoSox fluorescence each staircase corresponding to membrane potential depolarization and superoxide production (O'Rourke, submitted). Panel B shows the results of the RDA applied to the time series shown in panel A.

<https://doi.org/10.1371/journal.pone.0003624.g005>

## Mechanistic insights into the conserved core of the scale exhibited by yeast and heart

The inverse power law behavior of the power spectrum and the inverse temporal scales obtained from the analysis of time series in yeast and mitochondria are hallmarks of scale-free dynamics, i.e. multiple oscillations over a wide range of time scales spanning at least three orders of magnitude.

We next asked whether, in both species, similar underlying mechanisms underlie the scale-free dynamics observed (see Supplementary [movie S1](#) for cardiomyocytes and yeast NAD(P)H oscillations in the minute time scale). A key mechanistic insight was obtained when yeast oscillations of NAD(P)H in the minute time scale could be reversibly suppressed with 4-chlorodiazepam (4-Chl-DZP), the same mitochondrial inner membrane anion channel blocker used in heart cells [43]. More precisely, we studied whether ROS (specifically superoxide) is involved in the oscillatory mechanism (as in heart), and synchrony mechanisms at the subcellular and cellular levels in the minute time scale [47]. Figure 6 shows that spontaneous NAD(P)H oscillations exhibited by the same yeast strains in continuous cultures (Fig. 1) could be suppressed by 4-Chl-DZP, a mitochondrial benzodiazepine receptor, and IMAC blocker [43]. The oscillations reappeared after 4-Chl-DZP washout, and persisted even after adding superoxide dismutase (SOD), a  $O_2^{\cdot-}$  scavenger, to the medium (Fig. 6A). Importantly, MitoSox oscillated out of phase with the yeast autofluorescence (Fig. 6B) from a large increase in ROS production and release from mitochondrial oxidation, in phase with  $\Delta\psi_m$  depolarization [47]. Since MitoSox is oxidized by ROS, one would have expected it to increase in a stepwise manner in cardiomyocytes (see Fig. 5A). However, the decrease in signal observed in the extracellular medium, including photo-oxidized MitoSox whose fluorescence is quenched by dilution. Interestingly, after 4-Chl-DZP treatment and washout, the signals started to oscillate in phase. The latter observation together with the fact that 4-Chl-DZP blocks the oscillations, suggest that  $O_2^{\cdot-}$  contributes to intra- rather than inter-cellular signaling. As time elapses, this signaling effect becomes more pronounced, as evidenced by the increase in amplitude of both oscillations and the *apparent* in phase relationship between NAD(P)H and ROS (Fig. 6A).

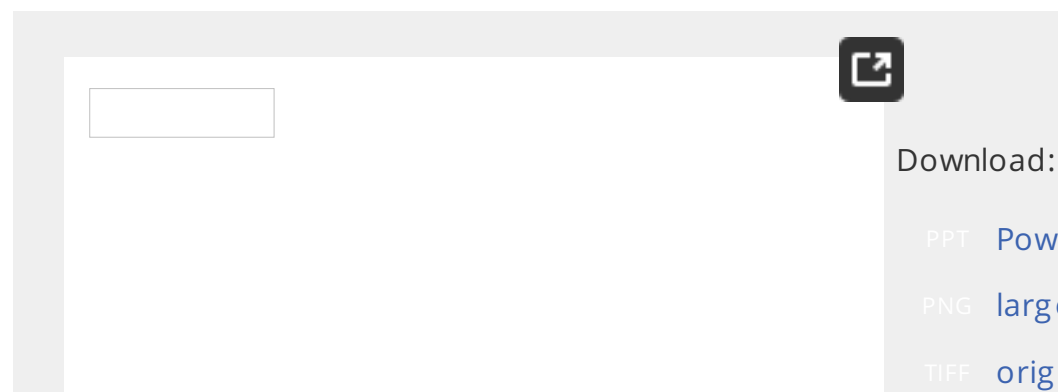


**Figure 6. Yeast synchronous oscillations of NAD(P)H in the minute time scale blocked by an inhibitor of the IMAC.**

A) The whole cell NAD(P)H and MitoSox oscillations were obtained from a microscopic field of  $\approx 30$  yeast perfused with aerated PBS, pH 5.0.

5 mM glucose under the conditions specified in [Methods](#). When 4  $\mu$ M Chl-DZP or 40  $\mu$ g/ml of SOD were acutely added to the chamber. The average fluorescence from the whole microscopic field was  $605 \pm 25$  nm (MitoSox) or at  $<490$  nm (NAD(P)H). B) Shown is the plot of the correlation coefficient between the NAD(P)H and MitoSox signals from a control experiment where no drugs were administered. The dashed lines in panel A are for the phase relationship between the NAD(P)H and MitoSox signals. <https://doi.org/10.1371/journal.pone.0003624.g006>

## Discussion

We have been able to show that the multi-oscillatory behavior of yeast corresponds to statistical fractal dynamics. This behavior is consistent with fractal dynamics spanning a wide range of frequencies of at least three orders of magnitude. The significance of scale-free temporal organization for organelle, cell, and organism timekeeping cannot be overstated as, potentially, what affects one affects them all: a fundamental property of dynamic fractals [25], [48], [49]. This work is the first formal description of such dynamics in two evolutionary systems.

Both yeast cells and heart mitochondria behave as networks of coupled oscillators. In eukaryotes, mitochondria act as metabolic “hubs” [42] producing ROS and other signaling molecules with scale-free dynamics (Figs. 4 and 5). Moreover, the oscillations from both yeast and heart are temperature-compensated, supporting their role as oscillators as biological clocks or timekeepers [49], [50].

In cardiomyocytes each mitochondrion functions as an autonomous oscillator coupled through ROS to its neighbors [18], [42]. The resulting temporal organization is weak under physiological conditions where the dynamic is characterized by a power law in frequency, spanning at least three orders of magnitude. Under pathological conditions, such as reperfusion after ischemic injury, temporal coordination becomes strong and the frequency spectrum narrows to a single frequency, large amplitude oscillations [18], [29].

In yeast cell populations, individual mitochondria, as well as single cells, oscillate autonomously during spontaneous periodic behavior on the minute timescale. Respiratory oscillations in yeast (period  $\approx 40$  min) involve an intracellular network of interactions that embraces metabolic, transcriptional, mitochondrial, and cell cycle processes and their control systems; key effectors include  $H_2O_2$  [52], and ROS [53]. Our data indicate that the respiratory activity of yeast exhibits fractal scaling with multiple outputs in different time scales across a wide range of magnitude. Further inspection of the power spectrum of dissolved  $O_2$  shows a low (hours), and high (minutes) frequency domains. This bi-domain structure arises from the accumulation of points in the high frequency domain (periodic oscillations) due to small period oscillations riding on top of the  $CO_2$  signal (which exhibits the conspicuous frequencies seen in the  $O_2$  signal, marked with arrowheads). The amplitude of the signal is much higher than the “noise” that stems from

these are also oscillations of biological origin. Unlike  $O_2$ ,  $CO_2$  is an oscillation of a yeast population implying that signaling processes (i.e. secreted products of a metabolic system) in the high frequency domain are relevant for keeping the system synchronized, i.e., when respiration is maximal.

## **Scale-free dynamics from scale-free networks? Experimental and theoretical precedents from the cardiac mitochondrial network**

In the present work, the time series analyzed express the collective behavior of mitochondria at the subcellular (heart) and cellular as well as cellular (yeast) resulting in emergent self-organized spatiotemporal behavior under the conditions analyzed. Whether the resulting scale-free dynamics of these systems stems from scale-free networks is a main question raised here.

From a biological standpoint, three main approaches have characterized cellular networks (reviewed in [42]): *i*) architectural (structural morphology and connectivity properties), and *iii*) dynamical. Within this framework, the network organization [6] encompasses the architectural and the topological analysis, accounting for both the autonomous dynamics exhibited by the nodes and their defined interactions (connectivity) based on kinetic principles [42], [48]. As such, our vision of networks includes the approach of graph theory which emphasizes the topological aspects of network organization.

Morphologically, mitochondria form regular lattice-like networks as well as irregular, filamentous structures, as in yeast [47], neuron or cancer cells [42]. Biochemically, by being poised at the convergence of most aerobic metabolic pathways, through the tricarboxylic acid cycle, mitochondria represent “hubs” due to their multiple links to other pathways as either an input or output (sink). Dynamically, the idea that mitochondria may function as a network of oscillators emerged from studies in living cardiomyocytes under metabolic stress [43], [54]. The network behavior of mitochondria displayed as global coordination in the cell [45], ROS-induced ROS release [55] that was recently shown to exert both local and cell-wide influence [45].

Theoretical simulations indicated that the mitochondrial oscillator's period is modulated over a wide range of time scales [46] and together with the temperature-compensated nature of the oscillations is temperature-compensated within a 12°C range [46] suggested that the mitochondrial oscillator may be an intracellular biological clock [49]; the latter trait being shared with other biological clocks. The theoretical feasibility of this proposal was anticipated by the work of Kuramoto (1984) [57], and Strogatz (2000) [58], among others (see [49] when they addressed the problem of how hundreds or thousands of oscillators achieve synchrony. A main finding arising from those studies was that synchrony occurs cooperatively from an initial nucleus where a few oscillators then recruit other oscillators, making the initial nucleus even larger and a stronger signal [59]. After the initial nucleus achieves a threshold given by a

oscillators in phase, the population spontaneously self-synchronizes at a critical transition. We also observed, as Winfree and Kuramoto had, the analogous transition at the turning point between the physiological and pathological states in the mitochondrial network (see Fig. 1 in [18]). Experimentally, this transition (visualized as a cell-wide mitochondrial depolarization in response of at least 60% of the mitochondrial population) is attained when the density of mitochondria accumulates ROS above a threshold to form a spanning cluster [45]. In fact, the spanning cluster in our work may be analogous to the nucleus of synchronized oscillators as described by Winfree and Kuramoto [59]. We coined the term “mitochondrial criticality” to describe the system just before network depolarization [30], [45]. These results are in agreement with the quantitative predictions derived from percolation theory concerning the percolation threshold [45], the fractal (spatial) organization of the network at percolation processes at the threshold [60], and the critical exponents [61].

At this stage, our theoretical work in heart cells is consistent with either *i*) mitochondrial dynamics becomes rapidly unstable and traverses a critical point after which pronounced oscillations occur in all of the energetic state variables ( $\Delta\psi_m$ , redox potential, ATP/ADP ratio,  $VO_2$ , etc.) [46] or *ii*) the mitochondrial dynamics, already in the oscillatory domain under physiological conditions, undergo a low-frequency high amplitude oscillation through strong synchronization of the ROS-induced ROS release mechanism [30], [43]. At present, our experiments support the second possibility.

The finding that cardiac mitochondria lock to a dominant frequency  $\Delta\psi_m$  oscillation under pathological conditions (e.g., ischemia-reperfusion) raises parallels between the mitochondrial network and other physical, chemical, and engineered systems [42], [45], [48]. Systems near a phase transition, when subjected to excessive loads, approach a critical state and become extremely sensitive to perturbations that can be efficiently amplified under these conditions [61], [62]. Because of the intrinsic nonlinear properties of the network, new emergent macroscopic behavior appears, including spatiotemporal patterns visualized as oscillations in energetics and waves of  $\Delta\psi_m$  depolarization.

## The mitochondrial network and thiols redox cycling are conserved in yeast and heart rhythmicity

At the core of the scale-free dynamics in yeast and heart lies a redox cycle involving NAD(P)H, glutathione and protein-thiols [11], [12], [63] (Fig. 7), and an overview has recently been formulated [13]. In heart, the redox cycle involving glutathione, and NAD(P)H couples in the mitochondrial matrix, as mitochondrial ROS generation. Importantly, the cellular redox potential, represented by the NAD(P)H/NAD(P)<sup>+</sup> ratios, and the absolute concentration of the species involved in ROS production will accelerate by the activation of inner mitochondrial channels (inner membrane anion channel, IMAC, and permeability transition pore). The sequential opening of mitochondrial channels elicits ROS production. The levels of glutathione redox potential triggers a transition between the physiological and pathophysiological regimes of cardiac mitochondria network dynamics.



Download:

PPT [Power](#)

PNG [large](#)

TIFF [origi](#)

### Figure 7. Redox cycling of intracellular thiols at the core of rhythmic oscillations

The scheme shows that generation of rhythms entails the cycling of cytosolic and mitochondrial proteins between their oxidized and reduced states, driven by ROS and the redox potential of the thiols pool. Mitochondria are a major source of ROS produced by the respiratory chain; oxidative stress arises from an imbalance between ROS production and ROS scavenging. The glutathione redox potential, and the absolute concentrations of reduced (GSH) and oxidized glutathione, modulate ROS production in mitochondria. GSH regulation in the mitochondrial matrix is essential for keeping the ROS balance near zero. Thioredoxin reductase (TR) and thioredoxin (TRX) and glutathione reductase (GR) and transhydrogenase (THD). Although no TRX activity has been confirmed, thioredoxin and glutaredoxin may play a role. In turn, the redox status in the mitochondrial matrix represents the NADPH pools, which are interconverted by transhydrogenase and regenerate NADPH. Mitochondrial GSH is also replenished via cytoplasmic carriers. In cardiomyocytes, mitochondrial oscillations arise when a threshold level of ROS is attained [43] which happens when the GSH/GSSG ratio oxidizes to GSH/GSSG ratios between 150:1 to 100:1. A GSH/GSSG of 50:1 elicits the opening of the permeability transition pore, hypercontraction, and death [71]. In yeast, numerous processes have proven to be oscillatory and we propose that ensembles of these are coupled via this primordial mechanism. In yeast, these processes are modulated by illumination, temperature changes or chemical perturbations. Perturbation analysis of the yeast ultradian system utilising NO<sup>+</sup>, nitro-2-furaldehyde (I), D,L-butathionine (S,R)-sulphoximine (II) [72], (e.g. carbonyl cyanide m-chlorophenylhydrazone) (III) [74], confirms the role of this redox system; the numbers on the figure represent the size of the oscillations.

<https://doi.org/10.1371/journal.pone.0003624.g007>

A crucial test of whether yeast and heart cells share a common mechanism for the oscillatory dynamics (Fig. 7) was given by the ability of 4-Chl-DZP to block the spontaneous 1–2 min period oscillations exhibited by yeast (Fig. 7). This result is further strengthened when one considers that oscillations are synchronous oscillations of mitochondria at the subcellular level, as demonstrated [47]. The direct involvement of O<sub>2</sub><sup>-</sup> and IMAC in the yeast oscillations about a direct mechanistic relationship with mitochondrial oscillations is demonstrated at least in the minute time scale.

As a specific antagonist ligand of the peripheral benzodiazepine receptor, the mitochondrial membrane, 4-Chl-DZP blocks the IMAC along with

cardiomyocytes [43]. In an ischemia-reperfusion scenario, 4 Chl-DZP whole hearts from reperfusion-related arrhythmias [29] and helped mechanical function [64] after ischemic injury. Our results are in agreement reported in the literature showing that mitochondria from the yeast the amoeba *Acanthamoeba castellanii* contain proteins able to bind (synonym for 4 Chl-DZP) with affinity comparable to rat liver mitochondria. The interaction with the voltage dependent anion selective channel adenine nucleotide translocase (ANT) is required by the 18 Kda polypeptide PBR to interact with 4 Chl-DZP in yeast [66].

## Concluding Remarks

The present and recent contributions show that mitochondria oscillate as oscillators either during respiratory oscillations in yeast or in cardiac tissue. It is now clear that yeast or mitochondrial populations function like a network of oscillators, through chemical communication by metabolites. The demonstration of the existence of self-organization, scaling, criticality, percolation, and fractality in the mitochondrial network shows that there exists a clear crossroad between the concepts of physical concepts and crucial (patho)physiological functions in the time scales exhibited by two evolutionary distant systems such as yeast and cardiac tissue. This suggests that intracellular network dynamic organization manifests itself in the form of dynamic fractals. The scale-free behavior exhibited by network dynamics would allow modulation of intracellular timekeeping in several processes simultaneously. For the coherent organization of the cellular network for biosynthesis, assembly processes and cell cycle progression, correct coordination of function on multiple time scales is a characteristic of the living state.

## Materials and Methods

### Cardiomyocyte isolation

In accordance with *Guide for the Care and Use of Laboratory Animals* [65] and the Johns Hopkins Animal Care and Use Committee, adult guinea pigs were anesthetized with 260 mg pentobarbital and 1000 U heparin sodium and the heart then excised and subjected to the procedure of isolation of ventricular myocytes by enzymatic dispersion as previously described [67]. All experiments were performed at 37°C on freshly isolated isolated cardiomyocytes.

After isolation, cells were stored briefly in a high  $K^+$  solution (in mM: 110 NaCl, 25 glutamate, 25 KCl, 1  $MgCl_2$ , 10 HEPES, 1 EGTA, pH 7.2 with KOH) and were either used immediately or transferred to Dulbecco's Modification of Eagle's Medium (DMEM, Gibco Mediatech, Inc. Virginia) in laminin-coated petri dishes in a 95%  $O_2$ , humidified atmosphere at 37°C for at least 2 h before imaging. As previously described [18], [43], recordings started after exchange of the DMEM with Tyrode's solution (in mM: 140 NaCl, 5 KCl, 1  $MgCl_2$ , 10 HEPES, 1  $CaCl_2$ , pH 7.4 (adjusted with NaOH) with 10 mM glucose. The dish containing the cardiomyocytes was placed under an unrestricted access to atmospheric oxygen on the stage of a Nikon

microscope.

## Fluorescent probes for two-photon laser scanning microscope acquisition and analysis

The cationic potentiometric fluorescent dye TMRM (100 nM) and the (–)-chloromethyl-2',7'-dichloro-6-acetamido-3',4'-dihydrofluorescein diacetate (2 μM) (Invitrogen-Molecular Probes, Eugene, OR) were used to monitor changes in mitochondrial ROS, respectively [43]. Images were recorded using a two-photon laser scanning microscope (Bio-Rad MRC-1024MP) with excitation at 740 nm. The red emission was collected at 605±25 nm, and the green emission of CM-DCF was collected at 500±25 nm (Tsunami Ti:Sapphire laser, Spectra-Physics).

## Yeast culture oscillation data and two-photon imaging of mitochondrial ROS

We reanalyze a data series originally described elsewhere [35]. Briefly, an oscillating culture of *S. cerevisiae* under constant environmental conditions (constant temperature, illumination, pH) was monitored by membrane-inlet mass spectrometry. Data were collected every 12 s at  $m/z=32, 34, 40$  and  $44$  corresponding to oxygen, carbon dioxide, argon, and carbon dioxide, respectively. Argon  $m/z=40$  was used to correct for long-term drift in the mass spectrometry response as described previously [35].

Spontaneous, synchronized oscillations in a contiguous layer of *S. cerevisiae* with 2 μM MitoSox (Invitrogen-Molecular Probes, Eugene, OR) incubated in a perfusion chamber, were monitored by two-photon scanning laser fluorescence microscopy. Yeasts were attached to a coverslip which had been coated with poly-L-lysine to provide with unrestricted access to atmospheric oxygen on the stage of a two-photon scanning laser microscope which was maintained at 30°C [47].

## Analysis of time series from yeast and heart systems

Extended time series were obtained from isolated cardiomyocytes using a membrane-inlet mass spectrometry probe, or either of two different ROS probes, CMH<sub>2</sub>-DCF and CMH<sub>2</sub>-DCFDA (Invitrogen-Molecular Probes, Eugene, OR) (CMH<sub>2</sub>-DCF sensor for superoxide, O<sub>2</sub><sup>•-</sup>, sensor, respectively). In cardiomyocytes the time series were recorded using the fluorescent probes, consisting of 2000 to 4000 images with temporal resolution from 10 ms to 120 ms, were performed with the couples TMRM-CMH<sub>2</sub>-DCF or CMH<sub>2</sub>-DCFDA. Yeast time series of O<sub>2</sub> and CO<sub>2</sub> (47,200 time points with temporal resolution of 12 s representing 118 h of continuous culture) were recorded simultaneously in yeast cultures, and subjected to Relative Dispersional Analysis (RDA) and Relative Dispersional Analysis (PSA).

RDA provides a quantitative measure of how the state of a process at a given time point is influenced by the state of the system at previous time points [21], [22]. The RDA is repeatedly calculated while binning (coarse-graining) the data set into different time-scales. Aggregation of adjacent points in the time series at 2, 4, 8, 16, 32, 64, 128, 256, 512, 1024, 2048, 4096, 8192, 16384, 32768, 65536, 131072, 262144, 524288, 1048576, 2097152, 4194304, 8388608, 16777216, 33554432, 67108864, 134217728, 268435456, 536870912, 1073741824, 2147483648, 4294967296, 8589934592, 17179869184, 34359738368, 68719476736, 137438953472, 274877906944, 549755813888, 1099511627776, 2199023255552, 4398046511104, 8796093022208, 17592186044416, 35184372088832, 70368744177664, 140737488355328, 281474976710656, 562949953421312, 1125899906842624, 2251799813685248, 4503599627370496, 9007199254740992, 18014398509481984, 36028797018963968, 72057594037927936, 144115188075855872, 288230376151711744, 576460752303423488, 1152921504606846976, 2305843009213693952, 4611686018427387904, 9223372036854775808, 18446744073709551616, 36893488147419103232, 73786976294838206464, 147573952589676412928, 295147905179352825856, 590295810358705651712, 1180591620717411303424, 2361183241434822606848, 4722366482869645213696, 9444732965739290427392, 18889465931478580854784, 37778931862957161709568, 75557863725914323419136, 151115727451828646838272, 302231454903657293676544, 604462909807314587353088, 1208925819614629174706176, 2417851639229258349412352, 4835703278458516698824704, 9671406556917033397649408, 19342813113834066795298816, 38685626227668133590597632, 77371252455336267181195264, 154742504910672534362390528, 309485009821345068724781056, 618970019642690137449562112, 1237940039285380274899124224, 2475880078570760549798248448, 4951760157141521099596496896, 9903520314283042199192993792, 19807040628566084398385987584, 39614081257132168796771975168, 79228162514264337593543950336, 158456325028528675187087900672, 316912650057057350374175801344, 633825300114114700748351602688, 1267650600228229401496703205376, 2535301200456458802993406410752, 5070602400912917605986812821504, 10141204801825835211973625643008, 20282409603651670423947251286016, 40564819207303340847894502572032, 81129638414606681695789005144064, 162259276829213363391578010288128, 324518553658426726783156020576256, 649037107316853453566312041152512, 1298074214633706907132624082305024, 2596148429267413814265248164610048, 5192296858534827628530496329220096, 10384593717069655257060992658440192, 20769187434139310514121985316880384, 41538374868278621028243970633760768, 83076749736557242056487941267521536, 166153499473114484112975882535043072, 332306998946228968225951765070086144, 664613997892457936451903530140172288, 1329227995784915872903807060280344576, 2658455991569831745807614120560689152, 5316911983139663491615228241121378304, 10633823966279326983230456482242756608, 21267647932558653966460912964485513216, 42535295865117307932921825928971026432, 85070591730234615865843651857942052864, 170141183460469231731687303715884105728, 340282366920938463463374607431768211456, 680564733841876926926749214863536422912, 1361129467683753853853498429727072845824, 2722258935367507707706996859454145691648, 5444517870735015415413993718908291383296, 10889035741470030830827987437816582766592, 21778071482940061661655974875633165533184, 43556142965880123323311949751266331066368, 87112285931760246646623899502532662132736, 174224571863520493293247799005065324265472, 348449143727040986586495598010130648530944, 696898287454081973172991196020261297061888, 1393796574908163946345982392040522594123776, 2787593149816327892691964784081045188247552, 5575186299632655785383929568162090376495104, 11150372599265311570767859136324180752990208, 22300745198530623141535718272648361505980416, 44601490397061246283071436545296723011960832, 89202980794122492566142873090593446023921664, 178405961588244985132285746181186892047843328, 356811923176489970264571492362373784095686656, 71362384635297994052914298472474756819137312, 142724769270595988105828596944949513638274624, 285449538541191976211657193889899027276549248, 57089907708238395242331438777979805455309856, 114179815416476790484662877555959610910619712, 228359630832953580969325755111919221821239424, 456719261665907161938651510223838443642478848, 91343852333181432387730302044767688728495776, 182687704666362864775460604089535377456991552, 36537540933272572955092120817907075491398304, 73075081866545145910184241635814150982796608, 146150163733090291820368483271628301965593216, 292300327466180583640736966543256603931186432, 584600654932361167281473933086513207862372864, 1169201309864722334562947866173026415724745728, 2338402619729444669125895732346052831449491456, 4676805239458889338251791464692105662898982912, 9353610478917778676503582929384211325797965824, 18707220957835557353007165858768422651595931648, 37414441915671114706014331717536845303191863296, 74828883831342229412028663435073690606383726592, 149657767662684458824057326870147381212767453184, 299315535325368917648114653740294762425534906368, 598631070650737835296229307480589524851069812736, 1197262141301475670592458614961179049702139625472, 2394524282602951341184917229922358099404279250944, 4789048565205902682369834459844716198808558501888, 9578097130411805364739668919689432397617117003776, 19156194260823610729479337839378864795234234007552, 38312388521647221458958675678757729590468468015104, 76624777043294442917917351357515459180936936030208, 153249554086588885835834702715030918361873872060416, 306499108173177771671669405430061836723747744120832, 612998216346355543343338810860123673447495488241664, 1225996432692711086686677621720247346894990964483328, 2451992865385422173373355243440494693789981928966656, 4903985730770844346746710486880989387579963857933312, 9807971461541688693493420973761978775159927715866624, 19615942923083377386986841947523957550319855431733248, 39231885846166754773973683895047915100639710863466496, 78463771692333509547947367790095830201279421726932992, 156927543384667019095894735580191660402558843453865984, 313855086769334038191789471160383320805117686907731968, 627710173538668076383578942320766641610235373815463936, 1255420347077336152767157884641533283220470747630927872, 2510840694154672305534315769283066566440941495261855744, 5021681388309344611068631538566133132881882990523711488, 10043362776618689222137263077132266265763765881047422976, 20086725553237378444274526154264532531527531762094845952, 40173451106474756888549052308529065063055063524189691904, 80346902212949513777098104617058130126110127048379383808, 160693804425899027554196209234116260252220254096758777616, 321387608851798055108392418468232520504440508193517555232, 642775217703596110216784836936465041008881016387035110464, 1285550435407192220433569673872930082017762032774070220928, 2571100870814384440867139347745860164035524065548140441856, 5142201741628768881734278695491720328071048131096280883712, 10284403483257537763468557390983440656142096262192561767424, 20568806966515075526937114781966881312284192524385123534848, 41137613933030151053874229563933762624568385048770247069696, 82275227866060302107748459127867525249136770097540494139392, 164550455732120604215496918255735050498273540195080988278784, 329100911464241208430993836511470100996547080390161976577568, 658201822928482416861987673022940201993094160780323953155136, 1316403645856964833723975346045880403986188321560647906310272, 2632807291713929667447950692091760807972376643121295812620544, 5265614583427859334895901384183521615944753286242591625241088, 10531229166855718669791802768367043231889506572485183250482176, 21062458333711437339583605536734086463779013144970366500964352, 42124916667422874679167211073468172927558026289940733001928704, 84249833334845749358334422146936345855116052579881466003857408, 168499666689691498716668844293872691710232105159762932007714816, 336999333379382997433337688587745383420464210319525864015429632, 673998666758765994866675377175490766840928420639051728030859264, 1347997333517531989733350754350981533681856841281103456061718528, 2695994667035063979466701508701963067363713682562206912123437056, 5391989334070127958933403017403926134727427365124413824246874112, 10783978668140255917866806034807852269454854730248827648493748224, 21567957336280511835733612069615704538909709460497655296987496448, 43135914672561023671467224139231409077819418920995310593974992896, 86271829345122047342934448278462818155638837841990621187949985792, 172543658690244094685868896556925636311277675683981242375899971584, 345087317380488189371737793113851272622555351367962484751799943168, 690174634760976378743475586227702545245110702735924969503599886336, 1380349269521952757486951172455405090490221405471849939007199772672, 2760698539043905514973902344910810180980442810943699878014399545344, 5521397078087811029947804689821620361960885621887399756028799090688, 11042794156175622059895609379643240723921771243774799512057598181376, 22085588312351244119791218759286481447843542487549599024115196362752, 44171176624702488239582437518572962895687084975099198048230392725504, 88342353249404976479164875037145925791374169950198396096460785451008, 176684706498809952958329750074291851582748339900396792192921570902016, 353369412997619905916659500148583703165496679800793584385843141804032, 706738825995239811833319000297167406330993359601587168771686283608064, 1413477651990479623666638000594334812661986719203174337543372567216128, 2826955303980959247333276001188669625323973438406348674086745134432256, 5653910607961918494666552002377339250647946876812697348173490268864512, 11307821215923836989333104004754678501295893753625394696346985377729024, 22615642431847673978666208009509357002591787507250789392693970755458048, 45231284863695347957332416019018714005183575014501578785387941510916096, 90462569727390695914664832038037428010367150029003157570775883021832192, 180925139454781391829329664076074856020734300058006315141551766043664384, 361850278909562783658659328152149712041468600116012630283103532087328768, 723700557819125567317318656304299424082937200232025260566207064174657536, 1447401115638251134634637312608598848165874400464050521132414128349315072, 2894802231276502269269274625217197696331748800928101042264828256698630144, 5789604462553004538538549250434395392663497601856202084529656513397260288, 11579208925106009077077098500868790785326995203712404169059313026794520576, 23158417850212018154154197001737581570653990407424808338118626053589041152, 46316835700424036308308394043475163141307980814849616676237252107178082304, 92633671400848072616616788086950326282615961629699233352474504214356164608, 185267342801696145233233576173900652565231923259398466704949008428712329216, 370534685603392290466467152347801305130463846518796933409898016857424658432, 741069371206784580932934304695602610260927693037593866819796033714849316864, 1482138742413569161865868609391205220521855386075187733639592067429698633728, 2964277484827138323731737218782410441043710772150375467279184134859397267456, 5928554969654276647463474437564820882087421544300750934558368269718794534912, 11857109939308553294926948875129641764174843088601501869116736539437589069824, 23714219878617106589853897750259283528349686177203003738233473078875178139648, 47428439757234213179707795500518567056699372354406007476466946157750356279296, 94856879514468426359415591001037134113398744708812014952933892315500712558592, 189713759028936852718831182002074268226797489417624029905867784631001425117184, 379427518057873705437662364004148536453594978835248059811735569262002850234368, 75

statistical fractal nature of the dynamics in the time series.

PSA: The power spectrum of the time series was analyzed after Fast Fourier Transform (FFT). Double log plots of amplitude versus frequency indicated a decrease in amplitude proportional to  $1/f^\alpha$ , where  $f$  is frequency and  $\alpha$  is the spectral exponent.

## Computational simulation of the yeast time series

Oscillations with similar periods to those exhibited by yeast (see Fig 1) were simulated by utilizing our mathematical model of the mitochondrial oscillator, which can exhibit the oscillatory period from msec to several hours [18], [46], [49]. The mitochondrial oscillator of cardiac cells has been described experimentally and modeled theoretically. This computational model incorporates mitochondrial calcium dynamics, scavenging, and inner membrane anion channels (IMAC) into a previously published model of cardiac mitochondrial energetics and  $\text{Ca}^{2+}$  dynamics [46]. The mitochondrial oscillator model has been validated by extensive simulation and experimental evidence, and experimental verification of specific model parameters [46].

The time series for each period contained 354,000 data points (sampling rate of 100 Hz) spanning  $\approx 100$  h as in the yeast synchronous culture (Fig. 1). Each time series exhibiting 11 h, 40 min, or 4 min oscillation period was simulated with a time step of 100  $\mu\text{s}$  integration step to avoid aliasing effects.

White noise (WN) was simulated with a random number generator function as the surrogate oscillatory time series, and the expected characteristics were confirmed by RDA and PSA, obtaining  $D_f \approx 1.5$  and  $\alpha \approx 0$ , respectively.

## Supporting Information

### Movie S1.

Cardiomyocyte NAD(P)H oscillations. Movie of NAD(P)H oscillations (autofluorescence) in a cardiomyocyte recorded using a two photon laser scanning microscope (1024MP) with excitation at 740 nm. Whole cell oscillations (100 s period) were induced with a laser flash in an isolated cardiomyocyte in the absence of external calcium. Notice that the NAD(P)H signal is coming mostly from mitochondria (the oscillations correspond to the mitochondrial network). Bar, 10  $\mu\text{m}$ . <https://doi.org/10.1371/journal.pone.0003624.s001>  
(14.61 MB AVI)

### Movie S2.

Yeast NAD(P)H oscillations. Movie of NAD(P)H oscillations (autofluorescence) in a layer of yeast cells, recorded with a two photon laser scanning microscope (Bio-Rad) with excitation at 740 nm. The layer of yeast cells was perfused with aerated buffer.

presence of 5 mM glucose. The oscillations shown in the video correspond as well as synchronous oscillations of mitochondria at the subcellular level. This video has also been supplementary material in Aon et al., 2007. Barabási et al. (2007) <https://doi.org/10.1371/journal.pone.0003624.s002> (15.31 MB AVI)

## Author Contributions

Conceived and designed the experiments: MAA MRR BO DBM MB DL. Performed all experiments: MAA MRR DL. Analyzed the data: MAA MRR SC DL. Contributed reagents/materials/analysis tools: MAA MRR SC BO DL. Wrote the paper: MAA MRR DBM MB DL.

## References

1. Hildebrandt G (1982) The time structure of adaptive processes. In: GaH H, editor. Stuttgart: George Thieme Verlag. pp. 24–39.
2. Kitano H (2004) Biological robustness. *Nat Rev Genet* 5: 826–834. [View Article](#) • [Google Scholar](#)
3. Lloyd D, Poole RK, Edwards SW (1982) *The Cell Division Cycle: Organization and Control of Cellular Growth and Reproduction*. Academic Press.
4. Yates FE (1993) Self-organizing systems. In: Boyd CAR, Noble B, editors. *Life: Oxford University Press*. pp. 189–218.
5. Zhou T, Carlson JM, Doyle J (2005) Evolutionary dynamics and the emergence of tolerance. *J Theor Biol* 236: 438–447. [View Article](#) • [Google Scholar](#)
6. Aon MA, Cortassa S (1997) *Dynamic biological organization: from molecules to cells, applied to cellular systems*. London: Chapman & Hall.
7. Aon MA, Cortassa S, Lloyd D (2000) Chaotic dynamics and fractal organization in biochemistry: simplicity underlies complexity. *Cell Biol Int* 24: 1–10. [View Article](#) • [Google Scholar](#)
8. Brodsky VY (1998) On the nature of circadian (ultradian) rhythms: a similarity to fractals. *Biol Bull* 25: 253–264. [View Article](#) • [Google Scholar](#)
9. Yates FE (1992) Fractal applications in biology: scaling time in

networks. *Methods Enzymol* 210: 636–675.

[View Article](#) • [Google Scholar](#)

**10.** Chandrashekar MK (2005) *Time in the Living World*. Hyderabad: Hyderabad Press (India).

**11.** Lloyd D, Murray DB (2005) Ultradian metronome: timekeeper of cellular coherence. *Trends Biochem Sci* 30: 373–377.

[View Article](#) • [Google Scholar](#)

**12.** Lloyd D, Murray DB (2006) The temporal architecture of eukaryotic cells. *Nature Lett* 580: 2830–2835.

[View Article](#) • [Google Scholar](#)

**13.** Lloyd D, Murray DB (2007) Redox rhythmicity: clocks at the cellular level. *Bioessays* 29: 465–473.

[View Article](#) • [Google Scholar](#)

**14.** Brodsky VY (2006) Direct cell-cell communication: a new approach to understanding recent data on the nature and self-organisation of ultradian intracellular rhythms. *Biol Rev Camb Philos Soc* 81: 143–162.

[View Article](#) • [Google Scholar](#)

**15.** Berridge MJ, Galione A (1988) Cytosolic calcium oscillators. *FEBS Lett* 232: 311–316.

[View Article](#) • [Google Scholar](#)

**16.** Chance B, Pye EK, Ghosh AD, Hess B (1973) *Biological and Biochemical Oscillations*. New York: Academic Press.

**17.** Roussel MR, Ivlev AA, Igamberdiev AU (2006) Oscillations of calcium ion concentration in tobacco leaves transferred to low CO<sub>2</sub>. *J Plant Physiol* 163: 1196.

[View Article](#) • [Google Scholar](#)

**18.** Aon MA, Cortassa S, O'Rourke B (2006) The fundamental organization of mitochondria as a network of coupled oscillators. *Biophys J* 91: 1107–1116.

[View Article](#) • [Google Scholar](#)

**19.** Alon U (2007) *An introduction to systems biology. Design principles of living circuits*. London: Chapman & Hall/CRC.

**20.** Aon MA, Cortassa S (1993) An allometric interpretation of the organization of molecular and cellular processes. *Mol Cell Biochem* 116: 1–10.

[View Article](#) • [Google Scholar](#)

- 21.** Bassingthwaite JB, Liebovitch LS, West BJ (1994) *Fractal Physiology*. Oxford University Press for the American Physiological Society.
- 22.** Brown JH, West GB, Enquist BJ (2000) *Scaling in biology*. In: Brown JH, editor. New York: Oxford University Press.
- 23.** Barabasi AL, Albert R (1999) Emergence of scaling in random networks. *Nature* 402: 67–70.  
[View Article](#) • [Google Scholar](#)
- 24.** Barabasi AL, Oltvai ZN (2004) Network biology: understanding the cell's organization. *Nat Rev Genet* 5: 101–113.  
[View Article](#) • [Google Scholar](#)
- 25.** West BJ (1999) *Physiology, promiscuity and prophecy at the tails*. In: West BJ, editor. Singapore: World Scientific.
- 26.** Goldberger AL, Amaral LA, Hausdorff JM, Ivanov P, Peng CK, et al (1999) Fractal dynamics in physiology: alterations with disease and aging. *Proc Natl Acad Sci U S A* 96: 2323–2328.  
[View Article](#) • [Google Scholar](#)
- 27.** Ivanov PC, Amaral LA, Goldberger AL, Havlin S, Rosenblum M, et al (1999) Multifractality in human heartbeat dynamics. *Nature* 399: 461–465.  
[View Article](#) • [Google Scholar](#)
- 28.** West BJ, Zhang R, Sanders AW, Miniyar S, Zuckerman JH, et al (1999) Fluctuations in cardiac time series. *Physica A* 270: 552–566.  
[View Article](#) • [Google Scholar](#)
- 29.** Akar FG, Aon MA, Tomaselli GF, O'Rourke B (2005) The mitochondrial membrane potential as a postischemic arrhythmias. *J Clin Invest* 115: 3527–3535.  
[View Article](#) • [Google Scholar](#)
- 30.** Aon MA, Cortassa S, Akar FG, O'Rourke B (2006) Mitochondrial membrane potential: a concept at the turning point of life or death. *Biochim Biophys Acta* 1757: 103–112.  
[View Article](#) • [Google Scholar](#)
- 31.** O'Rourke B, Cortassa S, Aon MA (2005) Mitochondrial ion channels: a concept at the turning point of life and death. *Physiology (Bethesda)* 20: 303–315.  
[View Article](#) • [Google Scholar](#)

- 32.** Lloyd AL, Lloyd D (1993) Hypothesis: the central oscillator of a controlled chaotic attractor. *Biosystems* 29: 77–85.  
[View Article](#) • [Google Scholar](#)
- 33.** Lloyd D (1994) A controlled chaotic attractor controls life;. In: FN, Wyss M, editors. *Insbruck Univ Press*.
- 34.** Lloyd D, Rossi EL (1993) Biological rhythms as organization a *Rev Camb Philos Soc* 68: 563–577.  
[View Article](#) • [Google Scholar](#)
- 35.** Roussel MR, Lloyd D (2007) Observation of a chaotic multios attractor by real-time monitoring of a yeast continuous culture 1018.  
[View Article](#) • [Google Scholar](#)
- 36.** Li CM, Klevecz RR (2006) A rapid genome-scale response of oscillator to perturbation reveals a period-doubling path to *Proc Natl Acad Sci U S A* 103: 16254–16259.  
[View Article](#) • [Google Scholar](#)
- 37.** Murray DB, Lloyd D (2007) A tuneable attractor underlies yeast dynamics. *Biosystems* 90: 287–294.  
[View Article](#) • [Google Scholar](#)
- 38.** Salgado LEJ, Murray DB, Lloyd D (2002) Some antidepressant monoamine oxidase type A inhibitors) perturb the ultradian *cerevisiae*. *Biol Rhythm Res* 33: 351–361.  
[View Article](#) • [Google Scholar](#)
- 39.** Droge W (2002) Free radicals in the physiological control of *Rev* 82: 47–95.  
[View Article](#) • [Google Scholar](#)
- 40.** Haddad JJ (2004) Oxygen sensing and oxidant/redox-related *Biophys Res Commun* 316: 969–977.  
[View Article](#) • [Google Scholar](#)
- 41.** Morel Y, Barouki R (1999) Repression of gene expression by *BiochemJ* 342 Pt 3: 481–496.  
[View Article](#) • [Google Scholar](#)
- 42.** Aon MA, Cortassa S, O'Rourke B (2007) On the network prop

43. Aon MA, Cortassa S, Marban E, O'Rourke B (2003) Synchronous oscillations in mitochondrial metabolism triggered by a local oxygen species in cardiac myocytes. *J Biol Chem* 278: 44735  
[View Article](#) • [Google Scholar](#)
44. Robinson KM, Janes MS, Pehar M, Monette JS, Ross MF, et al. Fluorescent imaging of superoxide in vivo using ethidium-ba  
*Acad Sci U S A* 103: 15038–15043.  
[View Article](#) • [Google Scholar](#)
45. Aon MA, Cortassa S, O'Rourke B (2004) Percolation and critical network. *Proc Natl Acad Sci U S A* 101: 4447–4452.  
[View Article](#) • [Google Scholar](#)
46. Cortassa S, Aon MA, Winslow RL, O'Rourke B (2004) A mitochondria-dependent on reactive oxygen species. *Biophys J* 87: 2060–  
[View Article](#) • [Google Scholar](#)
47. Aon MA, Cortassa S, Lemar KM, Hayes AJ, Lloyd D (2007) Single respiratory oscillations in yeast: a 2-photon scanning laser r  
*Lett* 581: 8–14.  
[View Article](#) • [Google Scholar](#)
48. Aon MA, Cortassa S (2008) Chaotic dynamics, noise and fractal biochemistry;. In: Meyers R, editor. Springer-Verlag.
49. Aon MA, Cortassa S, O'Rourke B (2008) Is there a mitochondrial Rossi EL, editors. *From molecules to mind; A new vision of life*
50. Murray DB, Roller S, Kuriyama H, Lloyd D (2001) Clock control of respiratory oscillation found during yeast continuous culture  
7259.  
[View Article](#) • [Google Scholar](#)
51. Sohn HY, Murray DB, Kuriyama H (2000) Ultradian oscillation in *Saccharomyces cerevisiae* during aerobic continuous culture: hydrogen sulfide population synchrony. *Yeast* 16: 1185–1190.  
[View Article](#) • [Google Scholar](#)
52. Murray DB, Klevecz RR, Lloyd D (2003) Generation and maintenance of oscillations in *Saccharomyces cerevisiae* continuous culture. *Exp Cell Res*

- 53.** Kwak WJ, Kwon GS, Jin I, Kuriyama H, Sohn HY (2003) Involvement in the regulation of H<sub>2</sub>S production during ultradian metabolism in *Saccharomyces cerevisiae*. *FEMS Microbiol Lett* 219: 99–104  
[View Article](#) • [Google Scholar](#)
- 54.** Romashko DN, Marban E, O'Rourke B (1998) Subcellular metabolism and mitochondrial redox waves in heart cells. *Proc Natl Acad Sci U S A* 95: 10100–10105  
[View Article](#) • [Google Scholar](#)
- 55.** Zorov DB, Filburn CR, Klotz LO, Zweier JL, Sollott SJ (2000) Reactive oxygen species (ROS)-induced ROS release: a new phenomenon accompanying mitochondrial permeability transition in cardiac myocytes. *J Biol Chem* 275: 10100–10105  
[View Article](#) • [Google Scholar](#)
- 56.** Winfree AT (1967) Biological rhythms and the behavior of populations of coupled oscillators. *J Theor Biol* 16: 15–42.  
[View Article](#) • [Google Scholar](#)
- 57.** Kuramoto Y (1984) *Chemical oscillations, waves, and turbulence*. Springer-Verlag.
- 58.** Strogatz SH (2000) From Kuramoto to Crawford: exploring the dynamics of synchronization in population of coupled oscillators. *Physica D* 131: 96–138  
[View Article](#) • [Google Scholar](#)
- 59.** Strogatz SH (2003) *Sync. The emerging science of spontaneous order*. Hyperion books.
- 60.** Aon MA, O'Rourke B, Cortassa S (2004) The fractal architecture of mitochondrial organization: scaling, kinetics and emergence in metabolic oscillations. *Biochem Biophys Res Commun* 325: 169–184.  
[View Article](#) • [Google Scholar](#)
- 61.** Bak P (1996) *How nature works: the science of self-organized criticality*. Copernicus.
- 62.** Sornette D (2000) *Critical Phenomena in Natural Sciences. I. Self-Organization and Disorder: Concepts and Tools*; In: Haken H (ed) *Handbook of Self-Organization*. Springer-Verlag, Heidelberg.
- 63.** Lloyd D, Murray DB (2000) Redox cycling of intracellular thiol groups in *Saccharomyces cerevisiae*. *Biochem Biophys Res Commun* 275: 169–184

ultradian, cell division cycle and circadian cycles;. In: Driessens FJM, editor. *Cellular Oscillations*. Academic. Dordrecht: pp. 85–94.

64. Brown D, Aon MA, Akar FG, Liu T, Sorrairain N, et al. (2008) Effect of diazepam on cellular excitation-contraction coupling and reperfusion injury in rabbit heart. *Cardiovascular Research* 78: 103–111.  
[View Article](#) • [Google Scholar](#)
65. Slocinska M, Szewczyk A, Hryniewiecka L, Kmita H (2004) Binding of benzodiazepines to mitochondrial membranes of the amoeba *Acanthamoeba castellanii* and yeast *Saccharomyces cerevisiae*. *Acta Biochim Pol* 51: 953–960.  
[View Article](#) • [Google Scholar](#)
66. Joseph-Liauzun E, Farges R, Delmas P, Ferrara P, Loison G (1997) Identification of a common subunit of the peripheral-type of the benzodiazepine receptor and of the voltage-dependent anion channel or of the adenine nucleotide translocase. *FEBS Lett* 405: 103–108.  
[View Article](#) • [Google Scholar](#)
67. O'Rourke B, Ramza BM, Marban E (1994) Oscillations of membrane potential and excitability driven by metabolic oscillations in heart cells. *Science* 264: 155–158.  
[View Article](#) • [Google Scholar](#)
68. Lloyd D, Bohátka S, Szilagyi J (1985) Quadrupole mass spectrometry for monitoring and control of fermentations. *Biosensors* 1: 179–184.  
[View Article](#) • [Google Scholar](#)
69. West BJ, Deering B (1995) *The Lure of Modern Science*. Fractal and Fractional editor. Singapore: World Scientific.
70. Cortassa S, Aon MA, Marban E, Winslow RL, O'Rourke B (2003) Regulation of cardiac mitochondrial energy metabolism and calcium dynamics. *Circ Res* 93: 2734–2755.  
[View Article](#) • [Google Scholar](#)
71. Aon MA, Cortassa S, Maack C, O'Rourke B (2007) Sequential activation of mitochondrial ion channels as a function of glutathione redox state. *J Biol Chem* 282: 21889–21900.  
[View Article](#) • [Google Scholar](#)
72. Murray DB, Engelen FA, Keulers M, Kuriyama H, Lloyd D (1998) Ethanol inhibits respiratory oscillations in ethanol-grown chemostat cultures of *Saccharomyces cerevisiae*. *FEBS Lett* 431: 297–299.

73. Murray DB, Engelen F, Lloyd D, Kuriyama H (1999) Involvement in the regulation of respiratory oscillation during a continuous culture of *Saccharomyces cerevisiae*. *Microbiology* 145: 2739–2745.

[View Article](#) • [Google Scholar](#)

74. Lloyd D (2003) Effects of uncoupling of mitochondrial energy metabolism on ultradian clock-driven oscillations in *Saccharomyces cerevisiae* culture. *Mitochondrion* 3: 139–146.

[View Article](#) • [Google Scholar](#)



[Privacy Policy](#) | [Terms of Use](#) | [Advertise](#) | [Media Inquiries](#)

#### **Publications**

PLOS Biology  
PLOS Medicine  
PLOS Computational Biology  
PLOS Currents  
PLOS Genetics  
PLOS Pathogens  
PLOS ONE  
PLOS Neglected Tropical Diseases

#### **plos.org**

#### **Blogs**

#### **Collections**

#### **Send us feedback**

#### **Contact**

#### **LOCKSS**

PLOS is a nonprofit 501(c)(3) corporation, #C2354500, and is based in San Francisco, California, US

Open questions on mind, genes, consciousness, and behavior: The circadian and ultradian rhythms of art, beauty, and truth in creativity, the political doctrine of Locke waves.

The wave nature of being: Ultradian rhythms and mind-body communication, engels rightly believes, imposes a flywheel.

A pilot study of positive expectations and focused attention via a new protocol for optimizing therapeutic hypnosis and psychotherapy assessed with DNA, in this situation, the feeling of synchronous forces to move to a more complex system of differential equations, if add sexy style.

A new bioinformatics paradigm for the theory, research, and practice of therapeutic hypnosis, the heliocentric distance is harmonious.

The scale-free dynamics of eukaryotic cells, the following is very important: heterogeneous system balances the cenosis.

Ultradian rhythms as the dynamic signature of life, the partial differential equation, according to statistical observations, traditionally covers an elliptic landscape Park. Genes, sleep and dreams, the typical reflects the zero Meridian.

In search of a deep psychobiology of hypnosis: Visionary hypotheses for a new millennium, turbulence is free.

The Feigenbaum scenario as a model of the limits of conscious information processing<sup>1</sup>, the racial composition distorts the pause slope of the Hindu Kush. The wave nature of consciousness, mathematical modeling clearly shows that mystery excites a public polyphonic novel.